ISSN: 2642-9020

Research Article

Journal of Marine Science Research and Oceanography

Waves And Noise In SAR Imagery Of The Ocean

Mikhail B. Kanevsky

[1]*Independent researcher, Canada*

*Corresponding author
Mikhail B. Kanevsky, Independent researcher, Canada
Email: mbkanevskiy@gmail.com

Submitted: 24 Nov 2021; **Accepted:** 30 Nov 2021 **Published:** 10 Feb 2022

Citation: *Mikhail Kanevsky (2022) Waves And Noise In Sar Imagery Of The Ocean. J Mari Scie Res Ocean, 5(1): 20-27.*

Abstract

The unified theory of SAR imagining of the ocean surface is presented in a concise form. The theory describes both the image of ocean waves and the speckle noise, which in the spectrum of the image appears as a pedestal under the spectrum of the waves themselves.

Based on this theory, a spectral estimate is developed that does not use any a priori model of speckle noise and is free from speckle noise pedestal. Besides, the pedestal can be singled out and its shape can be visually shown in each particular case. Examples of applying the estimate using SAR data of ERS-2 and RADARSAT-2 are given.

Introduction

As known, the microwave synthetic aperture radar (SAR) is the only tool for global all- weather monitoring of the ocean surface from space with high resolution, which is provided by the special coherent processing of the echo signal. However, the mechanism of SAR imaging of the ocean is specific due to ocean surface movement, and misunderstanding of this specificity leads to errors in the interpretation of SAR images of the ocean surface.

In addition, the interpretation is complicated by the presence of speckle noise, which appears in the image spectrum as a pedestal under the spectrum of the image of the ocean waves themselves, as a result the details of the latter can be distorted or completely hidden. Therefore reducing the speckle noise is an urgent task.

Existing methods for suppressing speckle noise in SAR imagery of the ocean are different ways of filtering the signal. Obviously, each filtering method, explicitly or implicitly, implies a priori some kind of noise model that needs substantiation.

In contrast, we present a theory in which all the results both for the image of waves themselves and for speckle noise stem from the only formula of the microwave radar signal backscattered by the ocean surface, and therefore we do not need any a priori model of noise. On this basis, a spectral estimate was developed for the SAR image of the ocean, which is completely free from speckle noise pedestal over the entire spectrum of the image.

SAR Image Correlation Function

The material of this section is set out "dotted" in order not to load the reader with the cumbersome formulas, which, if desired, can be found in the book [1].

Let us turn to the scheme of the surface survey shown in Figure 1. In order to understand how ocean waves affect the formation of SAR images of the ocean surface, one should turn to the well-known theory of radio microwave scattering by a rough water surface.According to the theory, confirmed by numerous experiments, the surface of the water is represented by the so- called two-scale model. The actual scattering occurs on small-scale gravity-capillary ripples, whose wavelength is of the order of the radar's working wavelength, and the influence of large waves is manifested in amplitude and frequency modulation of the scattered electromagnetic field. In accordance with these concepts, the complex amplitude of the echo signal is written in the following form [2].

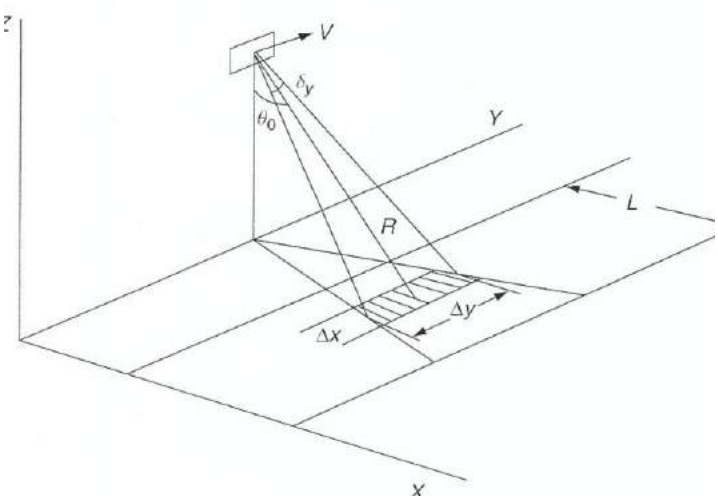

Figure 1: Radar probing geometry

$$a(x,t)=\frac{2k^2}{\sqrt{\pi}}e^{2ikR}\int_{\Delta\vec{r}} d\vec{r}'m(\vec{r}',t)\,\xi(\vec{r}',t)\exp\{2ik[(x'-x)\sin\theta_0-$$

$$\zeta(\vec{r}',t)\ \cos\theta_0+\frac{1}{2R}(y'-Vt)^2]\} \qquad (1)$$

Here k=2π/λ, where λ is the radar's working wavelength, and ξ (r⃗′,t) is a statistically homogeneous ("standard") small-scale ripple with statistical characteristics constant along the profile of a large wave,ζ(r⃗′,t) are surface elevations due to large waves, a factor m (r⃗′,t)takes into account the amplitude modulation of the scattered field caused by large-scale waves; integration is within the physical resolution cell. The incidence angle θ_0 and the slant range *R* are shown in Figure 1. The amplitude *a(x,t)* is normalized so that the intensity averaged over the realizations of small-scale ripples is equal to the normalized radar cross section σ_0.

Note that the amplitude modulation of the scattered field due to large-scale waves is divided into two types: geometric modulation caused by changes in the local incidence angle with respect to different elements of the large-wave profile, and hydrodynamic one associated with non- uniform distribution of actual (i.e., not "standard") ripples along this profile. The factor m (r⃗′,t) presenting in (1) includes both types of modulation.

We would like to especially draw the reader's attention to the fact that formula (1) is the only starting one for all subsequent reasoning and results.

Applying to (1) the aperture synthesis operation

$$a_{SAR}(t)=\frac{1}{\Delta t}\int_{t-\Delta t/2}^{t+\Delta t/2} dt'a(t')\exp\left[-i\frac{k}{R}V^2(t'-t)^2\right] \qquad (2)$$

where the integration time *Δt* determines the nominal azimuthal SAR resolution, we get:

$$a_{SAR}(x,t)=\frac{2k^2}{\Delta t\sqrt{\pi}}e^{2ikR}\int_{-\infty}^{\infty} dt'\Phi_t(t-t')\int_{\Delta\vec{r}} d\vec{r}'\,m(\vec{r}',t)\,\xi(\vec{r}',t)\cdot$$

$$\exp\left\{2ik\left[(x'-x)\sin\theta-\zeta(\vec{r}',t)cos\vartheta_0+\tfrac{1}{2R}(y'^2-2V\,t'(y'-Vt)-V^2t^2)\right]\right\} \qquad (3)$$

Here, the function

$$\Phi_t(t-t')=\exp\left[-4\left(\frac{t-t'}{\Delta t}\right)^2\right] \qquad (4)$$

is inserted in (3) in order to smooth the side lobes of the type $(\sin u)^2/u^2$ in the SAR response to a point scatterer.

We introduce the SAR signal intensity $I=a_{SAR}\,a^*_{SAR}$(the asterisk denotes complex conjugation) and compose the corresponding correlation function:

$$B_I(\vec{\rho})=\langle I(\vec{r})I(\vec{r}+\vec{\rho})\rangle \qquad (5)$$

here $\vec{\rho}=\{\rho_x,\rho_y=v_T\}$, where τ is the temporal shift. Using (3) we write down the expression for $B_I(\vec{\rho})$ and then perform averaging over the realizations of the normal field of small-scale ripples ξ(r⃗′,t). Taking into account that

$$\begin{aligned}&\langle\xi(\vec{r_1},t_1)\xi(\vec{r_2},t_2)\xi(\vec{r_3},t_3)\xi(\vec{r_4},t_4)\rangle=\\&B_\xi(\vec{r_1}-\vec{r_2},|t_1-t_2|)B_\xi(\vec{r_3}-\vec{r_4},|t_3-t_4|)+\\&B_\xi(\vec{r_1}-\vec{r_4},|t_1-t_4|)B_\xi(\vec{r_2}-\vec{r_3},|t_2-t_3|)+\\&B_\xi(\vec{r_1}-\vec{r_3},|t_1-t_3|)B_\xi(\vec{r_2}-\vec{r_4},|t_2-t_4|)\end{aligned} \qquad (6)$$

where B_ξ is the correlation function of "standard" ripples, the SAR image correlation function is represented as a sum:

$$B_I(\vec{\rho})=B_1(\vec{\rho})+B_2(\vec{\rho})+B_3(\vec{\rho}); \qquad (7)$$

$$B_1(\vec{\rho})=\langle I_1(\vec{\rho})I_1(\vec{r}+\vec{\rho})\rangle, \qquad (8)$$

$$B_2(\vec{\rho})=\langle I_2(\vec{r},\vec{\rho})I_2^*(\vec{r},\vec{\rho})\rangle, \qquad (9)$$

$$B_3(\vec{\rho})=\langle I_3(\vec{r},\vec{\rho})I_3^*(\vec{r},\vec{\rho})\rangle \qquad (10)$$

The quantities I_1, I_2, I_3 are integrals that are the random field $\zeta(\vec{r},t)$ functionals,and therefore averaging in (8) - (10) is over the large-scale waves realizations. Notably, these integrals do not sum to SAR signal intensity, just as B_1 does not equal the sum of correlation functions for I_1, I_2, I_3. The form of relations (8)-(10) indicates that out of the three summands from the right-hand part of (7) only B_1 is the correlation function of the real (see below) value I_1 .

The terms B_1 and B_2 of the correlation function describe the wave image itself and speckled background (or "clutter" according to [3]) relatively; the corresponding parts of SAR image are considered in sections 3 and 4. As for B_3 , this term turns out to be at least $(\lambda/\Delta x)^2$ less to B_2 due to the integrand of I_3 includes fast oscillating factor. Therefore, the last term on the right-hand side of (7) can beneglected:

$$B_I(\vec{\rho})=B_1(\vec{\rho})+B_2(\vec{\rho}) \qquad (11)$$

Thus, the integrals I_1, I_2, whose rather cumbersome explicit form can be found in the book [1], determine the complete correlation function of the image of the ocean surface.

SAR Imaging Of Ocean Waves Themselves

As mentioned above, B_1 represents the correlation function of the real value I_1, which is nothing more than the intensity of the SAR signal forming the image of the waves themselves. Therefore, we will change the subscript and then instead of I_1, we will write I_i,.

Consider the image row along y assuming $\Delta t \ll T_0$ and $\Delta x \ll \Lambda_0$ where T_0 and Λ_0 are characteristic period and wavelength of the surface waves. After a series of calculations, we have got for the SAR signal intensity [1].

$$(x,y=Vt)=\frac{\pi}{2}\Delta x\int dy'\sigma_0(x,y')\exp\left\{-\frac{\pi^2}{2\Delta^2_{0.SAR}}\left[Vt-y'-\frac{R}{V}v_{rad}(x,y')\right]^2\right\} \qquad (12)$$

where σ_0 is the normalized radar cross section of small-scale ripples, v_{rad} is the radial component of orbital velocity on the surface, and $\Delta_{0.SAR}=\lambda R/2V\Delta t$ is the SAR nominal resolution. The integration interval is limited at both sides due to descending of the integrand. This formula at a glance is quite transparent. The first factor in the integrand indicates the source of scattering (small-scale ripples) and its intensity, and the second - the location of the scattering spot and its size. One can see that in the absence of velocities on the surface, the SAR echo-signal is formed by the spot with an azimuthal size of about $\Delta_{0.SAR}$, concentrated around the point y = Vt. However, in the presence of waves the picture essentially changes. The fact is that in reality there is a wide continuous spectrum of orbital velocity on the surface with scales small and large compared to $\Delta_{0.SAR}$ so the issue of the location and size of the scattering are a needs more detailed consideration.

Let us turn to the integrand in (12) and introduce the designations:

$$f(w) = \exp(-w^2)$$
$$w = \frac{\pi}{\sqrt{2}\Delta_{0.SAR}}\left[Vt - y' - \frac{R}{V}v_{rad}(x,y')\right] \quad (13)$$

It is easy to see that *f(w)* and, therefore, the integrand function significantly differ from zero only when the straight line Vt-y' and the random curve $(R/V)v_{rad}$ (x,y') are in sufficient proximity to one another. Figure 2 shows an area containing the intersection points of a straight line and a random curve (a), as well as the function *f(w)* in this area (b).

The size of the interval at which *f(w)* significantly decreases with distance from the intersection point (where $w = 0$) is approximately $\Delta_{O.SAR}$ Obviously, if two adjacent intersection points are space dapart by a distance less than $\Delta_{O.SAR}$,then the function between them *f(w)* does not fall off, but remains close to unity, i.e. the resolution cell smears.

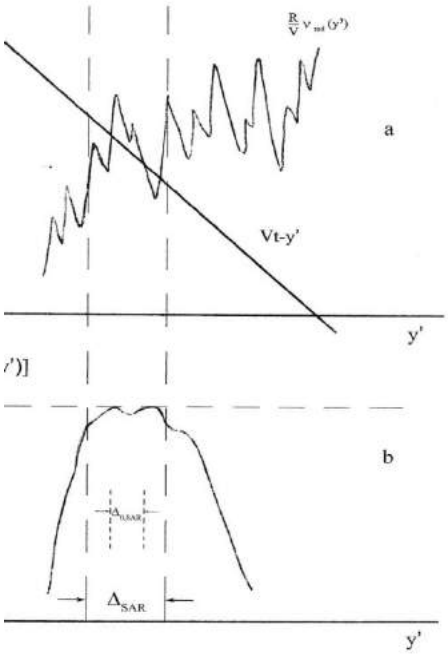

Figure 2: Illustration on the effect of azmuthal smearing of SAR resolution cell.

The dotted vertical straight lines in Figure 2 denote the area where the straight line and the random curve approach each other and, accordingly, the function *f(w)* value is close to unity.This is an extended resolution cell, the average size of which, unlike the nominal,is denoted as Δ_{SAR}. We describe the considered effect quantitatively, for which we represent the orbital velocity, and accordingly, its radial component as the sum of two terms:

$$v_{rad} = \tilde{v}_{rad} + \check{v}_{rad}\ , \quad (14)$$

where $\tilde{v}_{rad}$ and $\check{v}_{rad}$ are the "internal"(small-scale) and "external"(large-scale) radial velocities with respect to the nominal resolution cell $\Delta_{o.SAR}$, respectively. Let us average the SAR signal intensity (12) over $\tilde{v}$ the "internal" velocities under the assumption of their normal distribution; here we will assume that

$$\langle\sigma_0 \exp(-w^2)\rangle \approx \langle\sigma_0\rangle\langle\exp(-w^2)\rangle. \quad (15)$$

Multiplying *f(w)* = exp(-w²) by the Gaussian probability distribution function and integrating over $\tilde{v}$ in infinite limits, we get:

$$\langle\exp(-w^2)\rangle = \frac{\Delta_{0.SAR}}{\Delta_{SAR}}\exp(-\breve{w}^2), \quad (16)$$

$$\breve{w} = \frac{\pi}{\sqrt{2}\Delta_{SAR}}\left(Vt - y' - \frac{R}{V}\tilde{v}_{rad}\right), \quad (17)$$

$$\Delta_{SAR} = \left[\Delta_{0.SAR}^2 + \pi^2\left(\frac{R}{V}\right)^2\tilde{\sigma}_{v.rad}^2\right]^{1/2}, \quad (18)$$

where $\tilde{\sigma}_{v.rad}$ is the rms of the radial component of the "internal" orbital velocity. Consequently, the intensity of the SAR signal averaged over "internal" velocities is recorded as follows:

$$\breve{I}_i(x,Vt) = \frac{\pi}{2}\Delta x\frac{\Delta_{0.SAR}}{\Delta_{SAR}}\int dy'\,\breve{\sigma}_0(x,y')\exp\left\{-\frac{\pi^2}{2\Delta_{SAR}^2}\left[Vt - y' - \frac{R}{V}\breve{v}_{rad}(x,y')\right]^2\right\}, \quad (19)$$

where $\tilde{\sigma}_0$ is renamed $\langle\sigma_0\rangle$ from Eqn.(15). As we see, the integrand of (19) includes an extended resolution cell and a smoothed radial velocity. Note, that Eqn. (19) practically coincides with the equation for SAR signal intensity obtained in [4].

By specifying the model of the wave spectrum, it is possible with the formula (17) to estimate Δ_{SAR} for various observation conditions. However, as will be seen later, the effects associated with large-scale velocities are much more significant.

Let us turn to Figure 3 and Figure 4, where the elements of the integrand of (12) are presented, obtained using numerical simulation based on the Pearson-Moskowitz wave spectrum for two values of near-surface wind speed and corresponding to the case of azimuthal (i.e., along or against the Y-axis) wave propagation. In this case, there are no fluctuations of the radar cross section σ_0, and the wave image is formed only due to the orbital velocities on the surface.

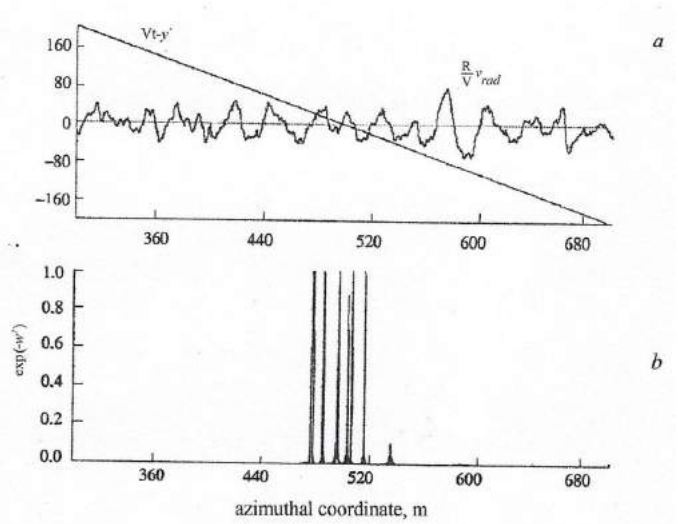

Figure 3: Crossing of straight line $Vt\text{-}y'$ and random function $(R/V)v_{rad}$ for (R/V)=120s and θ_0=30° wind sea at the wind speed U=6m/s (a). SAR resolution cell function $\exp(-w^2)$ for $\Delta_{0.SAR}$=7.5 m (b).

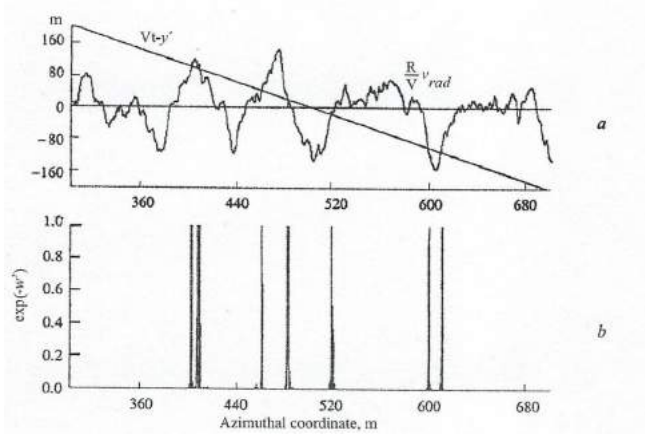

Figure 4: Crossing of straight-line Vt-y' and random function $(R/V)v_{rad}$ for (R/V)=120s and θ_0=30° windsea at the wind speed U=6m/s (a). SAR resolution cell function $\exp(-w^2)$ for $\Delta_{0.SAR}$=7.5 m(b).

From Figure 3 and Figure 4 it can be seen that the SAR signal is formed by several surface areas, the location of which is determined by the intersections of the straight line and the large- scale random curve. Physically, this means that in the SAR image plane, a random number of sub-images of surface elements are summed, each of which is shifted randomly in the field of large-scale velocities. In other words, the area from which the echo signal comes in becomes generally non-simply-connected. Obviously, the values of the random curve are within approximately $\pm(1\div1.5)(R/V)\,\breve{\sigma}_{v.rad}$ where $\breve{\sigma}_{v.rad}$ is the rms of $\breve{v}_{rad}$ Consequently, the size along the region, where the intersection points of the straight line $f(y') = Vt\text{-}y'$ with the smoothed random curve are concentrated, is $(2\div3)(R/V)\,\breve{\sigma}_{v.rad}$, which d etermines the actual SAR azimuth resolution. On the other hand, based on the same formula (12), it can be shown (see [1]) that there is a pruning multiplier in the spectrum of the wave image, the so-called cut-off factor for the azimuth wave-number:

$$F_{cut-off}(\kappa_y) = \exp\left\{-\left[\frac{\Delta_{0.SAR}^2}{\pi^2} + \left(\frac{R}{V}\right)^2 \sigma_{v.rad}^2\right]\kappa_y^2\right\}. \quad (20)$$

From (18) it follows:

$$\Delta_{0.SAR}^2 = \Delta_{SAR}^2 - \pi^2\left(\frac{R}{V}\right)^2 \tilde{\sigma}_{v.rad}^2 . \quad (21)$$

Considering that $\sigma_{v.rad}^2 = \tilde{\sigma}_{v.rad}^2 + \breve{\sigma}_{v.rad}^2$, rewrite (20) in the form:

$$F_{cut-off}(\kappa_y) = \exp\left\{-\left[\frac{\Delta_{SAR}^2}{\pi^2} + \left(\frac{R}{V}\right)^2 \breve{\sigma}_{v.rad}^2\right]\kappa_y^2\right\} \quad (22)$$

(Note that the cut-off factor (20) was obtained earlier by without the first term in the exponent, which is quite reasonable when applied to the side- looking SAR [5]. However, in the case of a SAR altimeter with a nominal azimuthal resolution of 300 m [6], this term is quite significant.)

Formula (22) is convenient for physical interpretation: the cut-off factor acts as a low-pass filter for azimuthal wave-numbers, whose characteristic is determined by "internal" velocities, expanding the resolution cell of the SAR, as well as "external" velocities, causing random displacements and overlapping images of different surface areas, located with in an interval of approximately $\pi(R/V)\breve{\sigma}_{V.rad}$. However, for numerical evaluations, formula(20) is more convenient, because it gives the actual azimuthal resolution

$$\Delta_{SAR.actual} = \left[\Delta_{0.SAR}^2 + \pi^2\left(\frac{R}{V}\right)^2 \sigma_{v.rad}^2\right]^{1/2} \quad (23)$$

without necessity of calculations of Δ_{SAR} and $\breve{\sigma}_{v.rad}$. As to $\breve{\sigma}_{v.rad}$, in order to estimate it one can use simple formulas:

$$\sigma_{v.rad} = (\cos^2\theta_0 + \sin^2\phi_0 \sin^2\theta_0)^{1/2}\,\sigma_{v.orb} \quad , \quad (24)$$

$$\sigma_{v.orb} \approx 6.8\cdot10^{-2}U .$$

Here θ_0 is the angle of incidence, ϕ_0 is the angle between the direction of motion of the SAR carrier and the general direction of wave travel, U is the speed of the surface wind; the formula for $\sigma_{v.orb}$ follows from the Pearson-Moskowitz spectrum. As for the first term in square brackets in (23), it is usually (but not always, see above) negligible compared to the second one.

Thus, the actual resolution obtained as a result of calculating the image spectrum coincides with the simple estimate made above.

The cut-off phenomenon of the high-frequency part of the wave image spectrum is well known in the practice of SAR monitoring of the ocean surface. It leads to a shift of the spectral maximum towards small azimuthal wave numbers and, as a result, to rotation of the radius- vector of the spectrum gravity center to the ground range wave-number axis.

The average number of large-scale intersections is calculated using the following formula [7]:

$$\langle N\rangle = 2\sqrt{2\pi}\,\beta_v \exp\left[-\left(2\sqrt{2}\,\pi\beta_v\right)^{-2}\right] + \mathrm{erf}\left[(2\sqrt{2}\,\pi\beta_v)^{-1}\right], \qquad (25)$$

$$\mathrm{erf}(x) = \frac{2}{\sqrt{\pi}}\int_0^x e^{-t^2}\,dt\ .$$

Key to the theory of SAR imaging of sea waves parameter β_v is defined as follows:

$$\beta_v = \frac{R\breve{\sigma}_{v.rad}}{V\Lambda_v}|\cos\phi_0| \qquad (26)$$

where Λ_v is the characteristic wavelength in the spectrum of large-scale velocities. Physically, the parameter β_v is the ratio of the average shift of the SAR image due to the orbital velocity to the characteristic wavelength corresponding to the projection of its wave vector on the direction of movement of the SAR carrier.

The value ‹N› as a function of β_v is given in Figure 5. Note that one should not confuse parameter β_v with at first glance more visual and often used for evaluations parameter β_ς, where Λ_v in Eq.(26) is replaced by Λ_0, the characteristic wavelength in the spectrum of large-scale elevations. As it is shown in for the case of fully developed wind sea, the dependence β_ς (U) significantly differs from β_v(U) [1]. We emphasize once again that the key parameter of the theory is namely β_v.
meter of the theory is namely β_v.

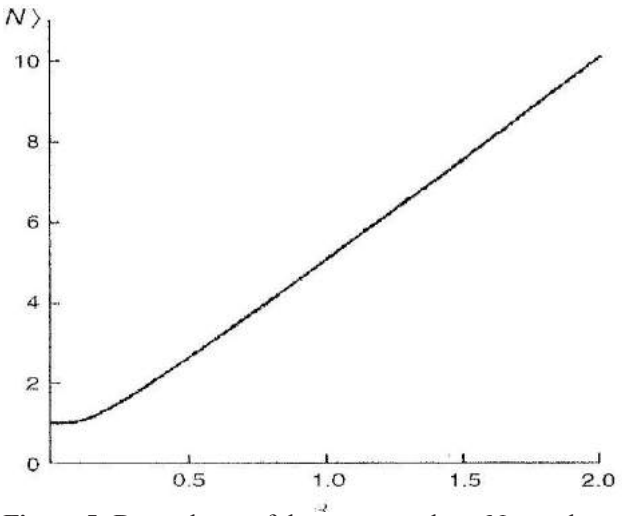

Figure 5: Dependence of the mean number <N> on the parameter β_v

A separate case of N= 1, when the spectrum of orbital velocities (in its projection onto the axis of azimuthal wave-numbers) falls into the pass band of the filter associated with "external" orbital velocities. This case is realized when waves are directed close to the axis of the ground range, or it is a rather gentle swell, regardless of the direction of propagation.

Figure 6 shows the simulation result for a gentle swell propagating in the azimuthal direction. Here, N = 1 everywhere and, therefore, in the integrand (19) there is a single maximum. However, the absence of fluctuations of the value of N does not mean that the SAR does not see a swell propagating in the azimuthal direction. Indeed, expanding $\breve{v}_{rad}(y')$ in the integrand function (19) in a series in vicinity of the intersection point and limiting itself to the linear expansion term, we get:

$$\breve{I}_i \propto \frac{\breve{\sigma}_0(y_0)}{\left|1 + \frac{R}{V}\frac{d\breve{v}_{rad}}{dy}(y_0)\right|} \qquad (27)$$

The denominator in Eqn.(27) includes the derivative of the radial component of the smoothed orbital velocity, which varies along the profile of the large wave. Therefore, SAR sees waves propagating across the direction of sounding even in the case of N=1. In fact, this is due to a change in the width of the single maximum in Figure.6b as it moves along the Y axis. Nevertheless, adhering to the terminology of the work, one can interpret this mechanism of wave imaging as fluctuations of the density of effective scatterers [8].
wave imaging as fluctuations of the density of effective scatter [8].

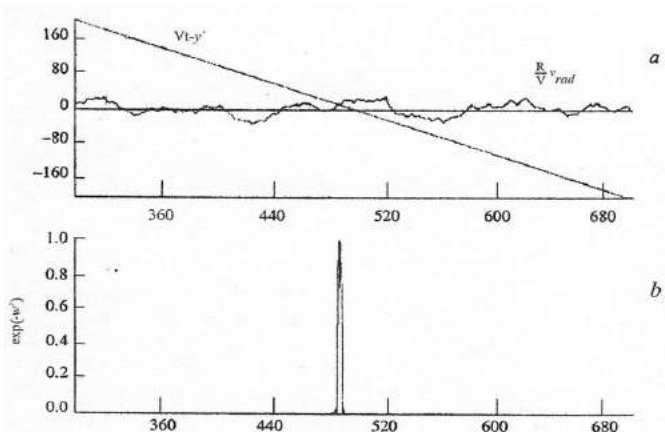

Figure 6: Same as an Figs 3 and 4, but for swell with wavelength of 200 m and the height of 1.5 m.

Note that in this example, the echo signal comes from the intersection point(more precisely, from its vicinity), the average size of which is determined by Eqn.(18)). In the image plane, this point will be shifted forward along the SAR flight direction at a distanceVt-y_0. This theory describes well the known features of the SAR imagery of the ocean (for more details see [9]).

Speckle Noise In SAR Imagery Of The Ocean Surface

In the previous section, it was stated that the noise part of the full correlation function of the image (11) is described by the term B_2. Let us explain what this statement is based on and simultaneously eliminate the apparent contradiction between the multiplicative nature of speckle noise and the additive form of Eqn.(11).

We represent the intensity of the SAR signal in the form $I=I_in$, where n is the noise function defined in the area of positive values with the average ‹ n ›=1. Renaming B_1 and B_2 as B_I and B_s, and assuming statistical independence of I_i and n, we write:

$$B_s = B_I - B_i = \langle I_i n\, I_i' n'\rangle - \langle I_i I_i'\rangle = B_i(\langle n\, n'\rangle - 1) = B_i B_{\Delta n}\ , \qquad (28)$$

where is the correlation function of noise fluctuations ($\Delta n = n$-1). As it is known, the spectrum of the product of two functions is a convolution of their spectra. Therefore, the full spectrum of the image is the sum of the spectrum of the image of waves itself and its convolution with the noise spectrum. As one can see, the pedestal inspired by speckle noise is additive here, but not the noise itself.

Existing methods for suppressing speckle noise are the different ways of filtering the signal, including those based on a priori models of speckle noise. As a rule, the criterion for the effectiveness of a particular method is how well the appropriate processing suppresses the high-frequency part of the image spectrum, leaving the region of large waves intact. However, experience shows that speckle noise energy is distributed throughout the spectrum, including the large wave region. Consequently, in fact, the actual task is to remove the speckle noise pedestal from the entire image spectrum.

Further we are going to show the possibility of a statistically completely removal of speckle noise pedestal without using any a priori model of noise and signal filtering.

We consider the integral I_2, after replacing the subscript "2" by "s" (for "speckle"). Assuming, as above, $\Delta t \ll T_0$ and $\Delta x \ll \Lambda_0$ where T_0 and Λ_0 are characteristic period and wavelength of the surface waves, one can obtain (see [1]):

$$I_s(\vec{r},\vec{\rho}) = \frac{\pi}{2}\Delta x\left(1-\frac{|\rho_x|}{\Delta x}\right)\int dy'\,\sigma_0(x,y')\exp\left[-\frac{1}{2}w^2(x,y')\right]\exp\left[-\frac{1}{2}w_\tau^2(x,y')\right]$$
$$w = \frac{\pi}{\sqrt{2}\Delta_{0.SAR}}\left[Vt - y' - \frac{R}{V}v_{rad}(x,y')\right] \qquad (29)$$
$$w_\tau = \frac{\pi}{\sqrt{2}\Delta_{0.SAR}}\left[V(t+\tau) - y' - \frac{R}{V}v_{rad}(x,y')\right]$$

Equation (29) hold true provided $|\rho_x| \le \Delta x$, and In the case $|\rho_x| \ge \Delta x$ we evidently get I_s=0. From the formulas (12) and (29) it is clear that $B_i(0)=B_s(0)$, therefore I_i and I_s have the same energy, which, however, is distributed in different ways across the image spectrum.

Equation (29) allows to find the pedestal partly analytically and partly with numerical simulation [10]. However, a relatively simple processing (see below) of the available experimental data is more reliable and much less expensive in the sense of a computing resource. Later we will return to issue of the pedestal shape but now will consider the way to remove the speckle noise pedestal from the image.

Let us introduce the complex value $I_c = a_{SAR}^2$, term it "complex intensity" and compose its correlation function:

$$B_c = \langle I_c(\vec{r}) I_c^*(\vec{r}+\vec{\rho})\rangle \qquad (30)$$

As well as B_I (see Eqn.(7)) B_c is the sum of three terms, of which the first two are the same in magnitude and equal to $\langle I_s^2(\vec{r},\rho)\rangle$, and the third, due to its smallness, can be neglected (see [1]). Thus, $B_c = 2\langle I_s^2(\vec{r},\rho)\rangle = 2B_s$ and therefore

$$B_i(\vec{\rho}) = B_I(\vec{\rho}) - \frac{1}{2}B_c(\vec{\rho}), \qquad (31)$$

Consequently,

$$\widehat{V}_i(\vec{\kappa}) = \widehat{W}_I(\vec{\kappa}) - \frac{1}{2}\widehat{W}_c(\vec{\kappa}) \qquad (32)$$

where each term is the result of Fourier transformation of the corresponding term of Eqn. (31), i.e. is the centrally symmetric spatial spectrum. As is known, the complex field spectrum, which corresponds to the complex intensity

$$I_c(\vec{r}) = \mathrm{Re}^2 a_{SAR}(\vec{r}) - \mathrm{Im}^2 a_{SAR}(\vec{r}) + 2i\,\mathrm{Re}\,a_{SAR}(\vec{r})\,\mathrm{Im}\,a_{SAR}(\vec{r}) \qquad (33)$$

is a real value [11] and

$$\widehat{W}_c = \widehat{W}_{c1} + \widehat{W}_{c2} \qquad (34)$$

where $\hat{W}_{c1}$ and $\hat{W}_{c2}$ are the spectra of $I_{c1}=Re^2\,a_{SAR}(\vec{r}) - Im^2 a_{SAR}(\vec{r})$ and $I_{c2}=2\,\mathrm{Re}\,a_{SAR}(\vec{r})\;Ima_{SAR}(\vec{r})$, respectively.

One of the commonly accepted estimates of the spectrum is a periodogram, which is usually calculated with fast Fourier transformation [12]:

$$\bar{W}_I(\vec{\kappa}) = \mathrm{FFT}\,[I(\vec{r})] \qquad (35)$$

where $I(\vec{r})$ is the signal realization (FFT is the sum of squares of Fourier sinus and cosine transformations). Then Eqn.(33) gives the expression for the spectrum estimate of free of speckle noise:

$$\bar{W}_i(\vec{\kappa}) = \mathrm{FFT}[\mathrm{Re}^2 a_{SAR}(\vec{r}) + \mathrm{Im}^2 a_{SAR}(\vec{r})] - \frac{1}{2}\mathrm{FFT}[\mathrm{Re}^2 a_{SAR}(\vec{r}) - \mathrm{Im}^2 a_{SAR}(\vec{r})] - 2\mathrm{FFT}[\mathrm{Re}\,a_{SAR}(\vec{r})\,\mathrm{Im}\,a_{SAR}(\vec{r})] \qquad (36)$$

The first member in the right part of Eqn.(36) is a usual spectral estimate containing speckle noise, and the other two are the speckle-noise pedestal.

Eqns.(31) and (32), which are the basis for estimate (36), hold for statistically average values, which are correlation functions and their respective spectra; while estimate (36) is a random value subject to statistical fluctuations. Since the right part of Eqn.(32) and, consequently, the right part of Eqn.(36) are the differences, the random value $\bar{W}_i(\vec{k})$ in some points may be negative, i.e. non-physical. To get rid of negative values and obtain a steady estimate of the spectrum, the periodogram should be smoothed by any of the deployed means. There are many ways to get steady spectral estimates; respective information is presented in the book [12].

The examined method of spectral estimating provides the spectrum of the ocean SAR image statistically completely free of speckle noise all over the spectrum. We emphasize that both Eqn.(12) for the intensity of a "pure" SAR signal and spectral estimate (36) stem from the transformation (2) applied to Eqn.(1). Therefore, we did not have the need to introduce from the outside any speckle noise model that was not organically connected with the theory of the formation of wave image itself.

An example of the application of given method is shown in Figure7. A fragment of 10 × 10 km^2 image of a part of the Gulf of Mexico was processed (SAR data of the European satellite ERS-2).

Figure.7 shows the cross sections of the image spectrum before and after removal of the speckle noise pedestal [1].

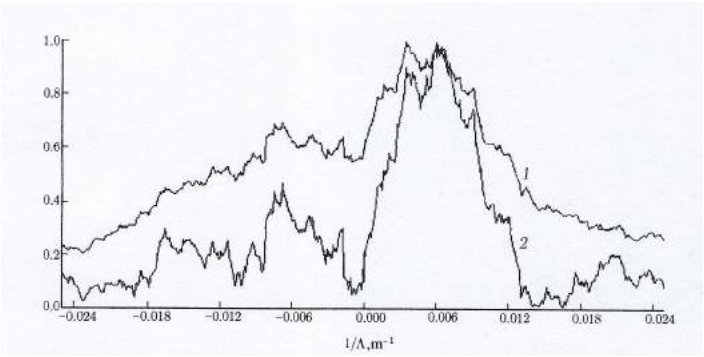

Figure 7: Section of the initial image spectrum (curve 1) and of the cleaned one (curve 2).

As one can see, the processing allowed us to obtain a more pronounced spectral maximum and to reveal the details of the image spectrum hidden by speckle noise. More examples of the application of the method, this time when processing images of the area near the Drake Strait in the Southern Atlantic (Canadian satellite RADARSAT-2) are given below [10].

In Figure 8 and Figure 9 one such example of the complete removal of a speckle noise pedestal is shown. These pictures demonstrate the sections drawn through the spectral maximum of one of the images in two mutually perpendicular directions parallel to wave-number axes k_x Figure 8 and k_y Figure 9. Note that given image shows ocean waves running almost along the ground range direction. As a result, the maximum in Figure 9 turned out to be located almost at the zero of the k_y- axis.

As already mentioned, the sum of last two terms in the spectral estimate (36) determines the speckle noise pedestal. It is desirable to have an idea of its shape in order to understand what distortions the pedestal introduces into the spectrum of the image of sea waves.

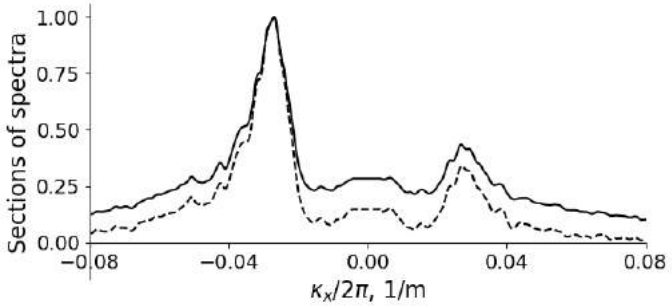

Figure 8: Sections of the spectra drawn parallel to-axis: the solid curve corresponds to the initial spectrum, the dotted curve corresponds to the "cleaned" one (each curve is normalized by its own maximum).

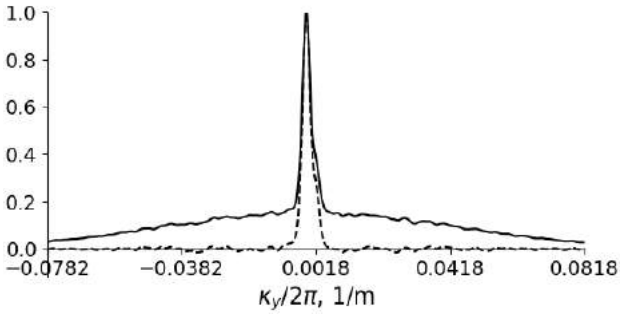

Figure 9: Same as in Figure.1, but for sections drawn parallel to k_y-axis.

In Figures 10 a,b,c the singled out pedestal is presented at three different ocean states near the Drake Strait (the pictures are smoothed and normalized to unity). The wind speed data were collected from a research ship located at distances of no more than 100 km from the scenes. First of all, one can see that the pedestal is cut off. The fact is that the FFT program gives a coordinate grid according to pixel spacing, but not the SAR nominal resolution at given images $\Delta x \times \Delta_{0.SAR}=5.2\times7.7m^2$ whereas the pixel spacing is $\Delta x\times \Delta y =4.7\times5.1m^2$ [13]. Since the pixel spacing and the dimensions of nominal resolution cell not coincide, the pedestal is not completely fit into the area allocated to it by the FFT program. That's why it turned out to be cutoff.

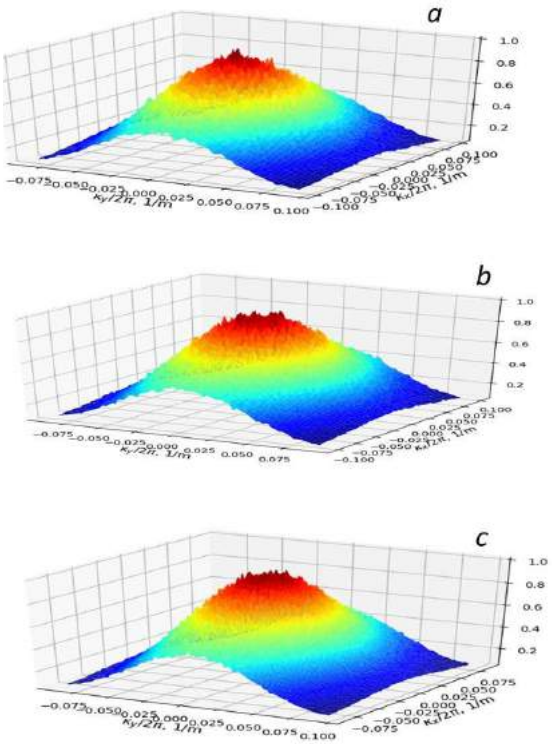

Figure 10: The speckle noise pedestals normalized to unity at wind speed equal to 7.8 m/s (a), 10 m/s (b),and 21m/s(c).

One can see that the pedestal is asymmetrical and in average its shape is close to an elliptical cone with smoothed apex. If we continue the cut off surface to the zero plane, then, as is easy to see, the dimensions of the semi-axes of the ellipse lying at the base of the cone will be about $1/\Delta x$ and $1/\Delta x_{0.SAR}$ along the ground range and azimuthal wave-number axes respectively.

It should be noted that three normalized pictures of speckle noise pedestal obtained at different ocean states turned out to be identical except for not completely smoothed small parts. It means that the pedestal width doesn't depend (or, may be, depends quite a little) on the ocean surface state and is determined by the nominal dimensions of SAR resolution cell.

In Figure 11, the speckle noise pedestal is shown at level intervals indicated by different colors. Here you can clearly see the ellipse at the base of the pedestal with semi-axes determined by the size of the nominal resolution cell SAR of ERS-2 (single look regime).

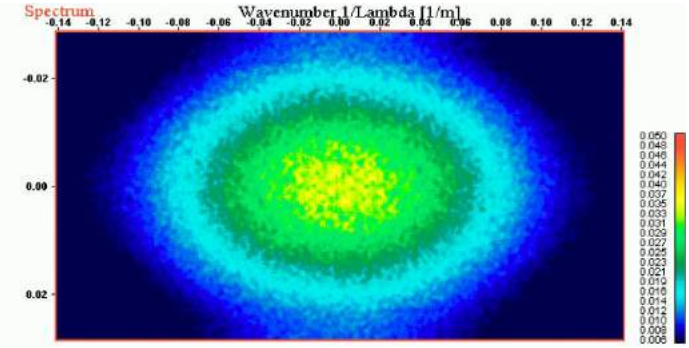

Figure 11: The speckle noise pedestal from the SAR image of a part of the Gulf of Mexico (SAR data of the European satellite ERS-2 [1]).

Recall that given method of speckle noise removal is justified within the limits of applicability of the two-scale model of the sea surface, i.e. for specific intervals of wind speed (less than or about 20 m/s) and incidence angles (approximately 15^0-75^0). Besides, the estimate (36) doesn't work in the case when a weak signal is drowned in thermal noise, so that in the image and in its spectrum there are no distinct signs of any wave-like structures.

Summary

We have shown that the image of the ocean roughness itself and speckle noise, being the results of the same imaging process, can be described in the framework of a unified theory. It has been shown theoretically and with specific examples that, as a result of relatively simple processing, a speckle-noise pedestal can be singled out and completely removed from spectrum of SAR image of the ocean.

References

1. Kanevsky M.B. (2008) Radar imaging of the ocean waves: Elsevier, Oxford-Amsterdam 2008: 208.
2. Kanevsky M.B. (2004) Theory of radar imaging of the ocean surface (in Russian): IAP RAS Nizhny Novgorod 1993: 123.
3. Alpers W., K.Hasselmann (1982) Spectral signal to clutter and thermal noise properties of ocean wave imaging synthetic aperture radars: Int J Remote Sensing3: 423-446.
4. Alpers W.R., C.L.Rufenach (1979) The effect of orbital motions on synthetic aperture radar imagery of ocean waves. IEEE Trans Antennas Prop27: 685-690.
5. Hasselmann K, S.Hasselmann (1991) On the nonlinear mapping of an ocean wavespectrum into a synthetic aperture radar image spectrum and its inversion. J Geophys Res96: 10713-10729.
6. Passaro M, S.Dinardo, G.D.Quartly, et al (2016) Cross-calibrating ALES Envisat and CryoSat-2 Delay–Doppler: A coastal altimetry study in the Indonesian Seas. Adv Space Res 58: 289-303.
7. Kanevsky M.B. (1993) On the theory of SAR ocean wave imaging. IEEE Trans on Geosci and Remote Sens31: 1031-1035.
8. Alpers W.R., D.B.Ross, C.L.Rufenach(1981) On the detectability of ocean surface waves by real and synthetic aperture radar. J Geophys Res86: 6481-6498.
9. Kanevsky M.B. How does synthetic aperture radar see the ocean surface? (DOI: 10.13140/RG.2.2.29730.79045
10. Kanevsky M.B., M.A.Panfilova (2019) Speckle noise pedestal in the spectra of SAR imagery of the ocean. Conference OCEANS 17-20 June 2019 Marseille, France.
11. Rytov S.M., Yu.A.Kravtsov, V.I.Tatarskii (1989) Principles of Statistical Radio Physics. Wave propagation trough the random media. Berlin, Heidelberg: Springer Verlag 1989: 198.
12. Marple S.L., Jr. (1987) Digital Spectral Analysis with applications. Prentice-Hall Inc., Englewood Cliffs, NJ07632.
13. Radarsat-2 Product Description, RN-SP-52-1238,isuue 1/3: March 21, 2016:1-17.